

2

MTL TR 89-58

AD

X-RAY DIFFRACTION ANALYSIS OF CONTROL AND TEST FIBERS

AD-A211 688

C. RICHARD DESPER
MATERIALS SCIENCE BRANCH

June 1989

Approved for public release; distribution unlimited.

DTIC
ELECTE
AUG 24 1989
S B D



US ARMY
LABORATORY COMMAND
MATERIALS TECHNOLOGY LABORATORY



89 8 24 097


U.S. ARMY MATERIALS TECHNOLOGY LABORATORY
Watertown, Massachusetts 02172-0001

The findings in this report are not to be construed as an official Department of the Army position, unless so designated by other authorized documents.

Mention of any trade names or manufacturers in this report shall not be construed as advertising nor as an official indorsement or approval of such products or companies by the United States Government.

DISPOSITION INSTRUCTIONS

Destroy this report when it is no longer needed.
Do not return it to the originator.



UNCLASSIFIED

SECURITY CLASSIFICATION OF THIS PAGE (When Data Entered)

Block No. 20

ABSTRACT

A series of fabric test panels, test fired with a 17-grain fragment simulating projectile (FSP), of armor materials made from Spectra 1000 (™Allied-Signal Corporation) high tenacity polyethylene fibers were examined by wide-angle X-ray diffraction. A new procedure was developed for averaging out the orientation of fiber or fabric samples in order to yield data suitable for the determination of crystallinity. Data on the undamaged fabric show an average crystallinity of 0.65, with an orthorhombic fraction of 0.61, and the metastable monoclinic phase fraction at 0.04. Ballistic impact resulted at the damage zone in either an increase in the monoclinic fraction, attributable to recrystallization, or to total eradication of the monoclinic phase, attributable to melting. Thus, the monoclinic content is useful for characterizing the thermomechanical effects which the fibers have undergone; monoclinic melting predominates when ballistic penetration is complete. The predominant orthorhombic phase is generally reduced in mass fraction by the ballistic impact event.

Accession For	
NTIS GRA&I	<input checked="checked" type="checkbox"/>
DTIC TAB	<input type="checkbox"/>
Unannounced	<input type="checkbox"/>
Justification	
By	
Distribution/	
Availability Codes	
Dist	Avail and/or Special
A-1	



UNCLASSIFIED

SECURITY CLASSIFICATION OF THIS PAGE (When Data Entered)

INTRODUCTION

X-ray diffraction analysis has been conducted on test panels of armor materials made from Spectra 1000™ polyethylene fibers of ultrahigh orientation. The focus to date has been on developing a test method for X-ray diffraction determination of crystallinity in the fibers using a suitable computer control method on the instrument to average out crystallite orientation. The method is described in detail in this report.

A total of 16 ballistically tested panels has been examined. Crystalline content was determined twice for each panel; once near the point of impact, and a second time at an undamaged area distant from the impact point.

The following diffraction peaks were observed: the monoclinic (001) reflection, near $2\theta = 19.4^\circ$, and the orthorhombic (110) and (200) reflections, near $2\theta = 21.5^\circ$ and 23.8° , respectively. In every instance, the equilibrium crystal form, the orthorhombic form, predominated, as evidenced by the strength of the peaks at 21.5° and 23.8° . The metastable monoclinic phase comprised a minor fraction of the crystalline material when it was present.

The monoclinic phase of polyethylene has been observed by a variety of workers: Slichter;¹ Seto, Hara, and Tanaka;^{2,3} Magill et al.;⁴ Fatou, Baker, and Mandelkern;⁵ and Mead, Desper, and Porter.⁶ In general, monoclinic material appears as the result of cold working of polyethylene; e.g. by compression or shear below the crystallizing melting point. The monoclinic phase is generally thought of as a metastable phase, less stable than the orthorhombic phase, to which it will transform under favorable conditions, such as heating near the melting point and removal of applied stress. The polymer molecular weight also plays an important role; higher molecular weights favor the formation of the monoclinic phase.

EXPERIMENTAL

The X-ray diffraction data were acquired using a specially modified Picker four-circle X-ray diffractometer at the U.S. Army Materials Technology Laboratory, as described by Desper.⁷ The system consists of the X-ray diffractometer, a PDP-11/23 computer for control of the four diffractometer angles, a position-sensitive proportional counter for detection, and a multiple-channel analyzer for data readout. Determination of crystallinities of fibrous materials presents a special problem, however, since the preferred crystallite orientation in the fibers results in a complicated diffraction pattern which is dependent upon both the usual Bragg angle 2θ and the fiber orientation angle χ . This was overcome by averaging out the orientation effect on the diffraction instrument (see Appendix 1) to reduce the data to patterns dependent upon only the angle 2θ , to which established methods for unoriented samples could be applied.

1. SLICHTER, W. P. *On the Morphology of Highly Crystalline Polyethylenes*. J. Polym. Sci., v. 21, 1956, p. 141-143.
2. SETO, T., HARA, T., and TANAKA, K. *Phase Transformation and Deformation Processes in Oriented Polyethylene*. Japan. J. Appl. Phys., v. 7, 1968, p. 31-41.
3. TANAKA, K., SETO, T., and HARA, T. *Crystal Structure of a New Form of High-Density Polyethylene, Produced by Press*. Japan., J. Phys. Soc., v. 17, 1962, p. 873-874.
4. MAGILL, J. H., POLLACK, S. S., and WYMAN, D. P. *Glass Temperature and Crystal Modification of Linear Polymethylene*. J. Polym. Sci. Pt. A, v. 3, 1965, p. 3781-3786.
5. FATOU, J. G., BAKER, C. H., and MANDELKERN, L. *The Effect of Crystallization Conditions and Temperature on the Polymorphic Forms of Polyethylene*. Polymer, v. 6, 1965, p. 243-248.
6. MEAD, W. T., DESPER, C. R., and PORTER, R. S. *The Physical and Mechanical Properties of Ultraoriented High-Density Polyethylene Fibers*. J. Polym. Sci., Polym. Phys. Edn., v. 17, 1979, p. 859-892.
7. DESPER, C. R. *An Advanced Technique for Characterization of Polymer Materials by Wide Angle X-ray Scattering in Materials Characterization for Systems Performance and Reliability*, J. W. McCauley and V. Weiss, ed., Plenum Press, NY, 1986, p. 319-337.

The X-ray beam has a circular cross section of 0.5-mm diameter and, at a monochromatic wavelength of 1.5418 Angstroms, is capable of penetrating the thickness of the test panel without serious absorption effects. Thus, the effective sample is a cylindrical section of fabric of 0.5-mm diameter, and of height equal to the fabric thickness. The beam diameter is considerably larger than the fiber yarn diameter, but a factor of 10 smaller than the 0.22 calibre projectile size. In all undamaged zone patterns, the target area of the X-ray beam was placed an inch from the damage zone and not along a warp or woof line with the point of impact. Damaged zone patterns were taken by placing the beam on fabric material as close as possible to the point of ballistic impact.

The raw data has been corrected by a Lorenz-polarization correction, which involves the diffraction instrument geometry and its systematic effect on measured intensities as a function of the Bragg angle 2θ . Further discussion of this correction is given in Appendix 2.

DETERMINATION OF PHASE CONTENT

We may define X_a , X_m , and X_o to be the mass fractions of amorphous, monoclinic, and orthorhombic phase material in the specimen, constrained to add up to unity. Our problem is then to calculate two of these mass fractions, using the X-ray diffraction data. Gopalan and Mandelkern⁸ provide a method for determining orthorhombic phase crystallinity in the absence of a monoclinic phase; we shall use this method to calculate the ratio X_a/X_o in the presence of the monoclinic phase. In this method, a straight line drawn through the Lorenz-polarization corrected data between the experimental intensities at $2\theta = 13^\circ$ and 27° is subtracted from the diffraction pattern. Finally, the areas of the crystalline peaks are mathematically separated from the background-corrected curve and denoted A_{001} , A_{110} , and A_{200} for the peaks mentioned above. The amorphous scattering area A_{am} is found by subtracting the three crystalline areas from the total area between 13° and 27° for the background-corrected curve.

The amorphous/orthorhombic ratio is found as in Gopalan and Mandelkern by:

$$R_a = X_a / X_o = A_{am} / (A_{110} + A_{200}).$$

Then the monoclinic/orthorhombic ratio is found from the ratio A_{001}/A_{110} using:

$$R_m = X_m / X_o = K_{fac} (A_{001} / A_{110})$$

where K_{fac} is a combined factor for structure factor, multiplicity, and temperature, and has the value 2.074. K_{fac} essentially corrects for the different intrinsic diffraction intensities of the monoclinic (001) and orthorhombic (110) planes.

Once these ratios are known, the three mass fractions are found in three simultaneous linear equations:

$$\begin{aligned} X_m &= R_m X_o, \\ X_a &= R_a X_o, \text{ and} \\ 1 &= X_a + X_o + X_m. \end{aligned}$$

8. GOPALAN, M. R., and MANDELKERN, L. *Degree of Crystallinity of Linear Polyethylene from Wide-Angle X-ray Diffraction*. *Polymer Letters*, v. 5, 1967, p. 925-929.

for which the solution is:

$$\begin{aligned} X_o &= 1 / (1 + R_a + R_m), \\ X_m &= R_m / (1 + R_a + R_m), \text{ and} \\ X_a &= R_a / (1 + R_a + R_m). \end{aligned}$$

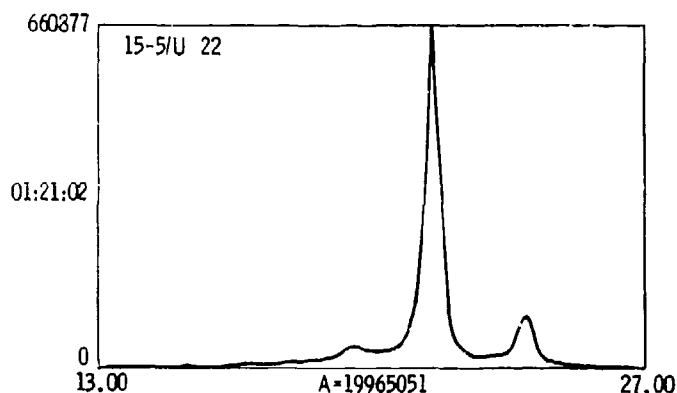
SAMPLE DATA

The sample data shall be presented in terms of the disk file name scheme used in data acquisition. Each data pattern identifies the sample, whether it was a complete or incomplete penetration, and whether a damaged or undamaged zone is being examined. The file name is eight characters, which of necessity begins with an alphabetical character, followed by the suffix .22, which indicates that $2\theta = 22.00^\circ$ is the center of the pattern. The letter C or I, indicating "complete" or "incomplete" penetration, is used as the first character. This is followed by the digits identifying a specific test panel sample, then either /D or /U to indicate that the X-ray beam is focused on a "damaged" or "undamaged" zone, respectively. Table 1 gives a list of the samples and the names of the corresponding patterns.

Table 1. CORRESPONDENCE BETWEEN SAMPLES AND DIFFRACTION PATTERNS

Sample Number	Penetration	Diffraction Pattern	
		Damaged Zone	Undamaged Zone
7-10-1	Complete	C10-1/D.22	C10-1/U.22
7-10-5	Complete	C10-5/D.22	C10-5/U.22
7-10-10	Complete	C10-10/D.22	C10-10/U.22
7-10-15	Complete	C10-15/D.22	C10-15/U.22
7-10-20	Complete	C10-20/D.22	C10-20/U.22
7-10-25	Complete	C10-25/D.22	C10-25/U.22
7-10-30	Complete	C10-30/D.22	C10-30/U.22
7-10-35	Complete	C10-35/D.22	C10-35/U.22
7-5-1	Incomplete	I5-1/D.22	I5-1/U.22
7-5-5	Incomplete	I5-5/D.22	I5-5/U.22
7-5-10	Incomplete	I5-10/D.22	I5-10/U.22
7-5-15	Incomplete	I5-15/D.22	I5-15/U.22
7-5-20	Incomplete	I5-20/D.22	I5-20/U.22
7-5-25	Incomplete	I5-25/D.22	I5-25/U.22
7-5-30	Incomplete	I5-30/D.22	I5-30/U.22
7-5-35	Incomplete	I5-35/D.22	I5-35/U.22

A typical diffraction pattern is shown in Figure 1. The pattern, as shown, has been subjected to the background and the Lorenz-polarization corrections. The vertical scale of the graph is X-ray counts, while the horizontal scale is the Bragg angle 2θ . The data acquisition time, 1 hour, 21 minutes, 2 seconds, is shown to the left of the graph. Below the graph, the peak search results from the multiple-channel analyzer, giving data from the three crystalline peaks (monoclinic [001], orthorhombic [110], and orthorhombic [200], reading left to right) evident in the pattern. The pertinent data items for each peak are the centroid, the central 2θ value of the peak in degrees; the FWHM, or line width (full width half maximum) of the peak in degrees; the peak count above baseline; and the net area of the peak in total counts. (Each peak has been fitted to a Gaussian curve and a baseline; the net area is that of the Gaussian curve.) These net area values are the data used for determination of the mass fractions of the two crystal phases. The percent area summary, shown further down in the figure, is not used. The amorphous area is found by subtracting the three resolved crystalline areas from the total area of the diffraction curve, indicated under the horizontal axis of the graph with the label $A=$. The calculated mass fractions of the crystalline and amorphous phases for the patterns are shown in detail in Table 2 and are summarized in Table 3.



Peak Search Report
(Full Analysis)

Peak	Centroid TTH	Left TTH	Right TTH	Peak Count	FWHM TTH	Area	Net Area
1	19.46	18.888	19.998	22481	4.561E-1	1.342E6	4.149E5
2	21.55	20.969	22.079	619232	4.479E-1	1.220E7	1.062E7
3	23.95	23.300	24.576	82526	5.016E-1	2.383E6	1.602E6

Percent Area Summary

Peak	Peak Area	Peak Area	Peak Net Area
	Area Between Cursors	Sum of Peak Areas	Sum of Net Areas
1	6.72	8.42	3.28
2	61.12	76.62	84.04
3	11.93	14.96	12.67

Figure 1. Typical corrected diffraction pattern.

Table 2. MONOCLINIC, ORTHORHOMBIC, AMORPHOUS CONTENT OF POLYETHYLENE FROM X-RAY DIFFRACTION

Sample	Input Areas				Corrected Mass Crystallinities		
	Mono. (001)	Ortho. (110)	Ortho. (200)	Total Area	Mono.	Ortho.	Total (Mono. + Ortho.)
C10-1/D.22	0	11970000	2716000	24060044	0.000	0.610	0.610
C10-1/U.22	261900	9402000	1124000	17024206	0.035	0.606	0.641
C10-5/D.22	0	1274000	223200	3565255	0.000	0.420	0.420
C10-5/U.22	241500	9549000	1431000	16706451	0.034	0.644	0.678
C10-10/D.22	193700	2712000	615200	6384188	0.074	0.498	0.572
C10-10/U.22	204400	9503000	1582000	16958468	0.029	0.643	0.671
C10-15/D.22	271400	6388000	1444000	14157003	0.047	0.537	0.585
C10-15/U.22	367700	8381000	1401000	16097223	0.054	0.589	0.642
C10-20/D.22	0	1851000	474100	4957032	0.000	0.469	0.469
C10-20/U.22	169800	7690000	1629000	14834582	0.028	0.617	0.646
C10-25/D.22	0	12800000	3505000	27034966	0.000	0.603	0.603
C10-25/U.22	223500	7213000	1022000	13720487	0.038	0.587	0.625
C10-30/D.22	0	7338000	1680000	16757360	0.000	0.538	0.538
C10-30/U.22	124300	7306000	1496000	13238413	0.023	0.656	0.679
C10-35/D.22	435700	3388000	635100	7481225	0.132	0.496	0.628
C10-35/U.22	407300	8035000	1303000	15059411	0.063	0.597	0.660
I5-1/D.22	0	3760000	904400	8971161	0.000	0.520	0.520
I5-1/U.22	206800	8846000	1616000	16501412	0.030	0.623	0.653
I5-5/D.22	672900	8493000	2139000	18541768	0.089	0.542	0.631
I5-5/U.22	414900	10620000	1602000	19965052	0.048	0.595	0.643
I5-10/D.22	158800	4808000	903900	9817222	0.039	0.568	0.607
I5-10/U.22	303700	8821000	1404000	16517419	0.043	0.603	0.647
I5-15/D.22	0	6150000	1512000	13057695	0.000	0.587	0.587
I5-15/U.22	198400	6804000	1142000	12512090	0.038	0.621	0.659
I5-20/D.22	164300	3943000	1048000	8743732	0.048	0.554	0.602
I5-20/U.22	248300	7001000	1106000	12815085	0.045	0.615	0.661
I5-25/D.22	1319000	16830000	4349000	40253760	0.081	0.500	0.581
I5-25/U.22	215500	7471000	1202000	13675321	0.037	0.620	0.658
I5-30/D.22	626200	6618000	1570000	16216661	0.094	0.481	0.576
I5-30/U.22	296000	7155000	1274000	13270735	0.053	0.615	0.668
I5-35/D.22	518900	4211000	785200	9778549	0.121	0.474	0.595
I5-35/U.22	218400	6480000	1140000	12397763	0.042	0.599	0.641

In the summary (Table 3), the mass fraction data are broken down into four classes for the four combinations of either complete or incomplete penetration and damaged or undamaged zones. Within each class, the average monoclinic and orthorhombic fractions are reported along with their respective standard deviations. Table 3 also includes the results of a replication experiment run to assess the reproducibility of the results. For this experiment, a single test specimen (7-5-5, incomplete penetration) was run at five different locations in its undamaged zone. The five different locations were used to assess the sampling effect, as well

as experimental uncertainty. The results for the replication experiment show a monoclinic fraction of 0.041 (standard deviation 0.006), and an orthorhombic fraction of 0.613 (standard deviation 0.021), for a total crystallinity of 0.654, and a standard deviation of 0.022.

Table 3. STATISTICAL ANALYSIS - MONOCLINIC FRACTION VALUES

Class	N	Monoclinic Fraction		Orthorhombic Fraction	
		Avg.	Std. Dev.	Avg.	Std. Dev.
Complete, Damaged	8	0.032	0.046	0.521	0.060
Complete, Undamaged	8	0.038	0.013	0.617	0.025
Incomplete, Damaged	8	0.059	0.042	0.528	0.039
Incomplete, Undamaged	8	0.042	0.006	0.611	0.010
Replicate	5	0.041	0.006	0.613	0.021

DISCUSSION

First of all, it should be noted that the results of all of the patterns of undamaged material are in essential agreement at a monoclinic fraction of 0.04 and an orthorhombic fraction of 0.61, with no statistically significant difference between the complete, undamaged and incomplete, undamaged classes. All undamaged material patterns may be regarded as representative of virgin fabric unaffected by the ballistic impact.

In the damaged classes, two effects are apparent. First of all, the monoclinic fraction shows gross fluctuations from sample-to-sample, ranging from zero to 0.132. Second, the orthorhombic fraction values are lower and show more fluctuation than the undamaged patterns. To illustrate the first effect, in the complete, damaged class, five of the eight patterns showed no monoclinic fraction, while the remaining three showed monoclinic fractions of 0.047, 0.074, and 0.132. Illustrating the second effect, orthorhombic fraction in that same class ranged from 0.420 to 0.610 for the eight patterns.

The changes in phase fractions brought about by the ballistic impact are regarded as arising from very localized heating of the fabric from the kinetic energy of the projectile. This heating can act in two ways. First, in the range of the well-known alpha transition of 90°C to 100°C, associated with the onset of molecular chain motion in the crystallites, crystallite growth and annealing is possible. Secondly, when the melting point around 140°C is exceeded, polymer will melt, then recrystallize to some extent in the quick cooling process.

For a number of the damaged patterns, evidenced by zero monoclinic content and quite low orthorhombic content, the melting process has predominated. In a few instances, where the monoclinic fraction well exceeds the undamaged value of 0.04, recrystallization has resulted in further growth of the monoclinic regions, perhaps at the expense of orthorhombic material, whose fraction generally drops with the ballistic event. (Recall that monoclinic polyethylene occurs, generally, in response to mechanical deformation.)

Overall, the complete, damaged class shows lower monoclinic fraction, and more instances of zero monoclinic fraction, than the incomplete, damaged class. This is taken to mean that when complete penetration occurs, melting predominates over recrystallization and, indeed, is probably associated with the failure of the material. Recrystallization is evident in the incomplete, damaged patterns in the fact that the average monoclinic fraction has increased to

0.059 over the undamaged value of 0.04. The increased scatter in the data for all of the damaged patterns is indicative of differences in the ballistic impact event from one test to the next.

While the monoclinic phase serves somewhat as a marker of thermomechanical history, the predominant phase in all patterns is the well-known orthorhombic phase. Both the complete, damaged, and incomplete, damaged classes show significant reduction in orthorhombic content compared to the undamaged fabric.

CONCLUSIONS

1. Polyethylene fabrics have been successfully characterized in terms of both monoclinic and orthorhombic crystal content by a suitable X-ray diffraction method.
2. Data on the undamaged fabric are consistent and show an average orthorhombic fraction of 0.61, and an average monoclinic fraction of 0.04.
3. Data from damaged fabric show that ballistic impact can result in either an increase in monoclinic fraction, attributed to recrystallization, or total eradication of monoclinic materials, attributed to melting. The latter predominates where ballistic penetration is complete.
4. Data from damaged fabric show that the major crystalline phase, the orthorhombic phase, is generally reduced in mass fraction by the ballistic impact event.
5. The monoclinic content of a polyethylene fabric is useful for characterizing thermomechanical effects which the fibers have undergone.

APPENDIX 1. FIBSCN PROGRAM FOR CRYSTALLINITY DETERMINATION

A Fortran program, FIBSCN, has been written for use in determining the crystallinity of fibers. The obstacle addressed and overcome by FIBSCN is the proper weighting of intensities at various orientation positions with respect to the fiber axis. A pertinent reference to this problem is Desper and Stein.⁹ Let us denote χ as the orientation angle between the fiber axis (presumed to be an axis of cylindrical symmetry) and the diffraction vector S of the diffractometer at a particular instrument setting. A weighting factor $\sin \chi$, herein termed the "Euler factor," must be used for proper integration and averaging over the surface of the sphere. With this definition, the randomized intensity $I_{ave}(2\theta)$ at any Bragg angle 2θ is given by:

$$I_{ave}(2\theta) = \int_0^{\pi/2} I(2\theta, \chi) \sin \chi \, d\chi / \int_0^{\pi/2} \sin \chi \, d\chi$$

where $I(2\theta, \chi)$ is the experimental intensity measured at the specified Bragg angle and orientation position. In effect, the above integration mathematically reduces the very complicated intensity pattern, which includes orientation dependence, to that of a hypothetical equivalent sample in which all of the scattering elements have been placed in random orientation positions. This reduces the crystallinity determination problem to one which has been extensively treated. The treatment used in the present work for polyethylene crystallinity is that of Gopalan and Mandelkern.⁸

The unique feature used for the first time in the present work is that of successfully coordinating the X-ray diffractometer with the use of a position-sensitive proportional counter (PSPC), which allows intensity to be measured over a considerable range of Bragg angles simultaneously rather than sequentially, with an enormous improvement in operational efficiency and reduction in data acquisition time. Without the PSPC, several days would be required to determine a single crystallinity for an oriented fiber; with the PSPC, this can be accomplished in 1 to 2 hours. FIBSCN takes the approach of applying the Euler factor $|\sin \chi|$ by varying the counting time which the diffractometer spends at each χ value directly with $|\sin \chi|$. Coordination of the two functions, motor positioning of the angle and data acquisition for the PSPC output, is accomplished by use of an auxiliary output signal, namely the "chart drive" logical signal, from the PDP-11 motor control system to gate the PSPC pulses to the Lecroy 3500 multiple-channel analyzer (MCA) where they are counted. The operation is as follows:

1. The PDP-11 drives to the next angle position with chart drive set **off** inhibiting PSPC pulse counting.
2. The PDP-11 turns chart drive **on** for a time proportional to $|\sin \chi|$, enabling PSPC pulse counting.
3. Repeat steps 1 and 2 for an entire quadrant of orientation angles.

The operator need only start the Lecroy 3500 MCA prior to step 1 and stop it after step 3. The intensity pattern recorded will be properly weighted to average out the orientation effect. The time indicated on the MCA will include angle driving time when pulse counting was inhibited, but this may be corrected in software after the fact by using a counting time value provided by the PDP-11.

9. DESPER, C. R., and STEIN, R. S. *Randomization of Orientation of Films and Fibers*. Polymer Letters, v. 5, 1967, p. 893-900.

APPENDIX 2. LORENZ-POLARIZATION CORRECTION

The Lorenz-polarization correction has been incorporated into the Lecroy 3500 multiple-channel analyzer software. This corrects for (a) the Lorenz instrumental geometry factor, which varies with the Bragg angle, and (b) the effect of polarization inherent in the diffraction processes. Note that two diffraction processes are relevant, those of both the incident beam monochromator, a graphite crystal selecting out the suitable X-ray wavelength, and of the sample diffraction process. With an incident beam monochromator of the Furnas designs used in the Picker diffractometer, the Lorenz-polarization factor L is given by:

$$L(2\theta, 2\theta_m) = (1 + \cos^2 2\theta / \cos^2 2\theta_m) / (\sin^2 \theta \cos \theta)$$

where

$$\begin{aligned} 2\theta &= \text{Bragg angle for sample scattering, and} \\ 2\theta_m &= \text{Bragg angle for monochromator crystal.}^{10} \end{aligned}$$

In this equation, the factor

$$1 / \cos^2 2\theta_m$$

corrects for the partial polarization of the monochromated incident beam. I use this form rather than

$$\cos^2 2\theta_m$$

given in Cullity¹⁰ and in most other texts because the design of the Picker instrument, with the monochromator bounce in a plane **perpendicular** to the sample scattering plane, gives an inverse primary beam polarization compared to the standard design in which the two planes are parallel.

10. CULLITY, B. D. *Elements of X-ray Diffraction*. Addison-Wesley, Reading, MA, 1956, p. 172.

DISTRIBUTION LIST

No. of Copies	To	No. of Copies	To
	Office of the Under Secretary of Defense for Research and Engineering, The Pentagon, Washington, DC 20301		Commander, U.S. Army Aviation Systems Command, P.O. Box 209, St. Louis, MO 63120-1798
1	ATTN: Mr. J. Persh	1	ATTN: AMSAV-NS, Mr. M. L. Bauccio
1	Dr. L. Young	1	Technical Library
1	Mr. K. R. Foster		Commander, U.S. Army Natick Research, Development, and Engineering Center, Natick, MA 01760
	Commander, U.S. Army Laboratory Command, 2800 Powder Mill Road, Adelphi, MD 20783-1145	1	ATTN: Technical Library
2	ATTN: AMSLC-IM-TL	1	Dr. J. A. Sousa
1	AMSLC-TD	1	Dr. R. J. Byrne
1	AMSLC-TD-A	1	Dr. R. Lewis
1	AMSLC-PA		Commander, U.S. Army Satellite Communications Agency, Fort Monmouth, NJ 07703
1	AMSLC-TP	1	ATTN: Technical Document Center
	Commander, Defense Technical Information Center, Cameron Station, Building 5, 5010 Duke Street, Alexandria, VA 22304-6145		Commander, U.S. Army Science and Technology Center Far East Office, APO San Francisco, CA 96328
2	ATTN: DTIC-FDAC	1	ATTN: Terry L. McAfee
1	National Technical Information Service, 5285 Port Royal Road, Springfield, VA 22161		Commander, U.S. Army Communications and Electronics Command, Fort Monmouth, NJ 07703
	Director, Defense Advanced Research Projects Agency, 1400 Wilson Boulevard, Arlington, VA 22209	1	ATTN: AMSEL-TDD, Mr. T. A. Pfeiffer, Technical Dir.
1	ATTN: Dr. P. Parrish		Director, Electronic Technology and Devices Lab, Fort Monmouth, NJ 07703
1	Dr. B. Wilcox	1	ATTN: DELET-D, Dr. C. G. Thornton
1	Dr. K. Hardmann-Rhyme		Commander, U.S. Army Tank-Automotive Command, Warren, MI 48397-5000
	Battelle Columbus Laboratories, Metals and Ceramics Information Center, 505 King Avenue, Columbus, OH 43201	1	ATTN: Dr. W. Bryzik
1	ATTN: Mr. W. Duckworth	1	D. Rose
1	Dr. D. Niesz	1	AMSTA-RKA
	Department of the Army, Office of the Assistant Secretary of the Army (RDA), Washington, DC 20310	1	AMSTA-UL, Technical Library
1	ATTN: Dr. J. G. Prather, Dep for Sci & Tech	1	AMSTA-R
1	Dr. J. R. Sculley, SARD	1	AMSTA-NS, Dr. H. H. Dobbs
	Deputy Chief of Staff, Research, Development, and Acquisition, Headquarters, Department of the Army, Washington, DC 20310		Commander, U.S. Army Armament, Munitions and Chemical Command, Dover, NJ 07801
1	ATTN: DAMA-ZE, Mr. C. M. Church	1	ATTN: Mr. J. Lannon
	Commander, U.S. Army Research and Development Office, Chief Research and Development, Washington, DC 20315	1	Mr. H. E. Peibly, Jr., PLASTEC, Director
1	ATTN: Physical and Engineering Sciences Division	1	Technical Library
	Commander, Army Research Office, P.O. Box 12211, Research Triangle Park, NC 27709-2211	1	Dr. T. Davidson
1	ATTN: Information Processing Office	1	Dr. B. Ebihara
1	Dr. J. Hurt		Commander, U.S. Army Armament, Munitions and Chemical Command, Rock Island, IL 61299
1	Dr. A. Crowson	1	ATTN: Technical Library
1	Dr. R. Reeber		Commander, U.S. Army Chemical Research, Development, and Engineering Center, Aberdeen Proving Ground, MD 21010-5423
1	Dr. R. Shaw	1	ATTN: SMCCR-TD, Mr. J. Vervier
	Commander, U.S. Army Materiel Command, 5001 Eisenhower Avenue, Alexandria, VA 22333		U.S. Army Corps of Engineers, Construction Engineering Research Lab, P.O. Box 4005, Champaign, IL 61820
1	ATTN: AMCQA-EQ, Mr. H. L. Light	1	ATTN: Dr. Robert Quattrone
1	AMCQA, Mr. S. J. Lorber		Commander, U.S. Army Belvoir RDE Center, Fort Belvoir, VA 22060-5606
	Commander, U.S. Army Materiel Systems Analysis Activity, Aberdeen Proving Ground, MD 21005	1	ATTN: STRBE-FS, Mr. W. McGovern, Fuel & Wtr Sup Div
1	ATTN: AMXSY-MP, H. Cohen	1	AMDME-V, Mr. E. York
	Commander, U.S. Army Night Vision Electro-Optics Laboratory, Fort Belvoir, VA 22060	1	STRBE-ZTS, Dr. K. H. Steinbach, Office of the Chief Scientist
1	ATTN: CELNV-S, Mr. P. Travesky	1	AMDME-ZT, Mr. T. W. Lovelace, Tech Dir
1	DELNV-L-D, Dr. R. Ruser	1	Mr. M. Lepera
1	DELNV-D, Dr. L. Cameron		Director, U.S. Army Ballistic Research Laboratory, Aberdeen Proving Ground, MD 21005
	Commander, Harry Diamond Laboratories, 2800 Powder Mill Road, Adelphi, MD 20783	1	ATTN: SLCBR-BLT, Dr. A. M. Dietrich
1	ATTN: Technical Information Office	1	SLCBR-BLF, Dr. A. Niller
1	SLCHD-RAE		Commander, Rock Island Arsenal, Rock Island, IL 61299
	Director, U.S. Army Research & Technology Labs, Ames Research Center, Moffet Field, CA 94035	1	ATTN: SARRI-EN
1	ATTN: DAVDL-D, Dr. R. Carlson		Director, U.S. Army Industrial Base Engineering Activity, Rock Island, IL 61299
1	DAVDL-AL-D, Dr. I. C. Statler, MS215-1, Aeromechanics Laboratory	1	ATTN: AMXIB-MT, Mr. G. B. Ney
	Commander, U.S. Army Missile Command, Redstone Scientific Information Center, Redstone Arsenal, AL 35898-5241		Commander, U.S. Army Chemical Research, Development and Engineering Center, Aberdeen Proving Ground, MD 21010-5423
1	ATTN: AMSMI-RD-CS-R/Doc	1	ATTN: AMSMC-CLD(A), Dr. B. Richardson
1	AMSMI-R, Dr. W. C. McCorkle		

No. of Copies	To	No. of Copies	To
1	Commander, U.S. Army Test and Evaluation Command, Aberdeen Proving Ground, MD 21005	1	National Aeronautics and Space Administration, Langley Research Center, Hampton, VA 23665
1	ATTN: AMSTE-ME	1	ATTN: Mr. J. Buckley, MS 387
1	AMSTE-TD, Mr. H. J. Peters	1	Dr. J. Heyman, MS 231
		1	Mr. R. L. Long, MS 266
1	Commander, U.S. Army Foreign Science and Technology Center, 220 7th Street, N.E., Charlottesville, VA 22901	1	Commander, White Sands Missile Range, Electronic Warfare Laboratory, OMEW, ERADCOM, White Sands NM 88002
1	ATTN: Military Tech	1	ATTN: Mr. Thomas Reader, AMSEL-WLM-ME
1	Mr. J. Crider		
1	Ms. P. Durrer		
1	Mr. P. Greenbaum		
1	Chief, Benet Weapons Laboratory, Watervliet, NY 12189	1	Department of Energy, Division of Transportation, 20 Massachusetts Avenue, N.W., Washington, DC 20545
1	ATTN: AMDAR-LCB-TL	1	ATTN: Dr. R. J. Gottschall, ER-131, GTN
1	Dr. G. D'Andrea		
1	AMDAR-LCB, Dr. F. Sautter	1	Mechanical Properties Data Center, Belfour Stulen Inc., 13917 W. Bay Shore Drive, Traverse City, MI 49684
1	Commander, U.S. Army Aviation Systems Command, Aviation Research and Technology Activity, Aviation Applied Technology Directorate, Fort Eustis, VA 23604-5577	1	National Institute of Standards and Technology, Washington, DC 20234
1	ATTN: SAVDL-MOS	1	ATTN: E. S. Etz, Bldg. 222, Rm A-121
		1	D. L. Hunston, Bldg. 224, Rm A-209
		1	Dr. D. H. Reneker, Dep. Dir., Ctr for Mat'l's Sci.
		1	Dr. Lyle Schwartz
		1	Dr. Stephen Hsu
		1	Dr. Allan Draggoo
1	Project Manager, Munitions Production Base, Modernization and Expansion, Dover, NJ 07801	1	U.S. Bureau of Mines, Mineral Resources Technology, 2401 E. Street, N.W., Washington, DC 20241
1	ATTN: AMCPM-PBM-P	1	ATTN: Mr. M. A. Schwartz
1	Technical Director, Human Engineering Laboratories, Aberdeen Proving Ground, MD 21005-5001	1	National Institute of Standards and Technology, Gaithersburg, MD 20899
1	ATTN: SLCHE-D, Dr. J. O. Weisz	1	ATTN: Dr. S. Wiederhorn
		1	Dr. N. Tighe
1	Chief of Naval Research Arlington, VA 22217		
1	ATTN: Code 471	1	National Research Council, National Materials Advisory Board, 2101 Constitution Avenue, Washington, DC 20418
1	Dr. A. Diness	1	ATTN: Dr. K. Zwilsky
1	Dr. R. Pohanka	1	D. Groves
		1	J. Lane
1	Naval Research Laboratory, Washington, DC 20375		
1	ATTN: Code 5830		
		1	National Science Foundation, Materials Division, 1800 G Street, N.W., Washington, DC 20006
1	Headquarters, Naval Air Systems Command, Washington, DC 20360	1	ATTN: Dr. L. Toth
1	ATTN: Code 5203	1	Dr. J. Hurt
1	Headquarters, Naval Sea Systems Command, 1941 Jefferson Davis Highway, Arlington, VA 22376	1	AVCO Corporation, Applied Technology Division, Lowell Industrial Park, Lowell, MA 01867
1	ATTN: Code 035	1	ATTN: Dr. T. Vasilos
1	Headquarters, Naval Electronics Systems Command, Washington, DC 20360	1	Case Western Reserve University, Department of Metallurgy, Cleveland, OH 60605
1	ATTN: Code 504	1	ATTN: Prof. A. H. Heuer
1	Commander, Naval Ordnance Station, Louisville, KY 40214	1	Defence Research Establishment Pacific, FMO, Victoria, B.C., VOS 1B0, Canada
1	ATTN: Code 85	1	ATTN: R. D. Barer
1	Director, Naval Industrial Resources Support Activity, Building 75-2, Room 209, Naval Base, Philadelphia, PA 19112-5078	1	Ford Motor Company, Turbine Research Department, 20000 Rotunda Drive, Dearborn, MI 48124
1	Commander, Naval Weapons Center, China Lake CA 93555	1	ATTN: T. Whelan
1	ATTN: Mr. F. Markarian		
		1	Ford Motor Company, P.O. Box 2053, Dearborn, MI 48121
1	Commander, U.S. Air Force Wright Aeronautical Labs, Wright- Patterson Air Force Base, OH 45433	1	ATTN: Dr. D. Compton, Vice President Research
1	ATTN: Dr. N. Tallan		
1	Dr. H. Graham	1	General Electric Company, Research and Development Center, Box 8, Schenectady, NY 12345
1	Dr. R. Ruh	1	ATTN: Dr. R. J. Charles
1	Aero Propulsion Labs, Mr. R. Marsh	1	Dr. C. D. Greskovich
1	Dr. H. M. Burt	1	Dr. S. Prochazka
1	AFMIL/MLLP, Mr. D. Forney		
1	AFMIL/MLLM, Mr. H. L. Gegel	1	Georgia Institute of Technology, EES, Atlanta, GA 30332
1	AFSC/MLLM, Dr. A. Katz	1	ATTN: Mr. J. D. Walton
1	Commander, Air Force Armament Center, Eglin Air Force Base, FL 32542	1	GTE Sylvania, Waltham Research Center, 40 Sylvania Road, Waltham, MA 02154
1	ATTN: Technical Library	1	ATTN: Dr. W. H. Rhodes
1	National Aeronautics and Space Administration, Lewis Research Center, 21000 Brookpark Road, Cleveland, OH 44135	1	Martin Marietta Laboratories, 1450 South Rolling Road, Baltimore, MD 21227
1	ATTN: J. Accurio, USAMKDL	1	ATTN: Dr. J. Venables
1	Dr. H. B. Probst, MS 49-1		
1	Dr. S. Dutta	1	Massachusetts Institute of Technology, Department of Metallurgy and Materials Science, Cambridge, MA 02139
1	NASA - Scientific and Technical Information Facility, P.O. Box 8757, Baltimore/Washington International Airport, Maryland 21240	1	ATTN: Prof. R. L. Coble
		1	Prof. H. K. Bowen
		1	Prof. W. D. Kingery
		1	Prof. J. Vander Sande

No. of Copies	To
1	Materials Research Laboratories, P.O. Box 50, Ascot Vale, VIC 3032, Australia ATTN: Dr. C. W. Weaver
1	Midwest Research Institute, 425 Volker Boulevard, Kansas City, MO 64110 ATTN: Mr. G. W. Gross, Head, Physics Station
1	Pennsylvania State University, Materials Research Laboratory, Materials Science Department, University Park, PA 16802 ATTN: Prof. R. Roy
1	Prof. R. E. Newham
1	Prof. R. E. Tressler
1	Dr. C. Pantano
1	Mr. C. O. Ruud
1	State University of New York at Albany, Department of Physics, Albany, NY 12222 ATTN: Prof. W. A. Lanford
1	State University of New York at Stony Brook, Department of Materials Science, Long Island, NY 11790 ATTN: Prof. F. F. Y. Wang
1	Stanford Research International, 333 Ravenswood Avenue, Menlo Park, CA 94025d ATTN: Dr. P. Jorgensen
1	Dr. D. Rowcliffe
1	United Technologies Research Center, East Hartford, CT 06108 ATTN: Dr. J. Brennan
1	Dr. K. Prewé
1	University of California, Lawrence Livermore Laboratory, P.O. Box 808, Livermore, CA 94550 ATTN: Mr. R. Laidingham
1	Dr. C. F. Cline
1	Dr. J. Birch Holt
1	University of Florida, Department of Materials Science and Engineering, Gainesville, FL 32611 ATTN: Dr. L. Hench
1	University of Washington, Ceramic Engineering Division, FB-10, Seattle, WA 98195 ATTN: Prof. R. Bradt
1	Westinghouse Electric Corporation, Research Laboratories, Pittsburgh, PA 15235 ATTN: Dr. R. J. Bratton
1	Rensselaer Polytechnic Institute, Department of Materials Engineering, Troy, NY 12181 ATTN: R. J. Diefendorf
1	Oak Ridge National Laboratory, P.O. Box X Oak Ridge, TN 37830 ATTN: P. F. Becher
1	V. J. Tennery
2	R. Johnson
1	Sandia Laboratories, Albuquerque, NM 87185 ATTN: Dr. F. Gerstle, Div 5814
1	The John Hopkins University, Department of Civil Engineering/ Materials Science and Engineering, Baltimore, MD 28218 ATTN: Dr. R. E. Green, Jr.
1	Director, Office of Science and Technology Policy, Old Executive Office Building, Washington, DC 20223

No. of Copies	To
1	Subcommittee on Science, 2319 Rayburn House Office Building, Washington, DC 20515 ATTN: Mr. P. C. Maxwell
1	Aerospace Corporation, Materials Science Laboratory, 2350 East El Segundo Boulevard, El Segundo, CA 90245 ATTN: Dr. L. R. McCreight
1	IBM Corporation, Thomas B. Watson Research Center, Yorktown Heights, NY 10598 ATTN: Dr. G. Onoda
1	Corning Glass Works, Research and Development Division, Corning, NY 14830 ATTN: Dr. W. R. Prindle
1	3M Company, New Products Department, 218-35-04, 3M Center, St. Paul, MN 55144 ATTN: R. E. Richards
1	Technology Strategies, Inc., 10722 Shingle Oak Ct., Burke, VA 22015 ATTN: Dr. E. C. Van Reuth
1	Rutgers University, Center for Ceramics, Rm A274, P.O. Box 909, Piscataway, NJ 08854 ATTN: Prof. J. B. Wachtman, Jr., Director
1	Syracuse University, 304 Administration Building, Syracuse, NY 13210 ATTN: Dr. V. Weiss
1	Lehigh University, Materials Research Center #32, Bethlehem, PA 18015 ATTN: Dr. D. M. Smyth
1	Alfred University, New York State College of Ceramics, Alfred, NY 14802 ATTN: Dr. R. L. Snyder
1	Alfred University, Center for Advanced Ceramic Technology, Alfred, NY 14802 ATTN: R. M. Spriggs
1	University of California, Center for Advanced Materials, 058, Hildebrand Hall, Berkeley, CA 94720 ATTN: Prof. G. Somorjai
1	Boeing Aerospace Company, 11029 Southeast 291, Auburn, MA 98002 ATTN: W. E. Strobelt
1	University of California, Materials Science and Mineral Engineering, Hearst Mining Building, Rm 284, Berkeley, CA 94720 ATTN: Prof. G. Thomas
2	Director, U.S. Army Materials Technology Laboratory, Watertown, MA 02172-0001 ATTN: SLCMT-TML
1	Author

<p>U.S. Army Materials Technology Laboratory Watertown, Massachusetts 02172-0001 X-RAY DIFFRACTION ANALYSIS OF CONTROL AND TEST FIBERS - C. Richard Desper</p>	<p>AD <u>UNCLASSIFIED</u> UNLIMITED DISTRIBUTION</p>
<p>Technical Report MTL TR 89-58, June 1989, 11 pp- illus.-tables, D/A Project: 1L161102.AH52</p>	<p>Key Words</p> <p>X-ray diffraction Body armor Filament fibers</p>
<p>A series of fabric test panels, test fired with a 17-grain fragment simulating projectile (FSP), of armor materials made from Spectra 1000 ("Allied-Signal Corporation) high tenacity polyethylene fibers were examined by wide-angle X-ray diffraction. A new procedure was developed for averaging out the orientation of fiber or fabric samples in order to yield data suitable for the determination of crystallinity. Data on the undamaged fabric show an average crystallinity of 0.65, with an orthorhombic fraction of 0.61, and the metastable monoclinic phase fraction at 0.04. Ballistic impact resulted at the damage zone in either an increase in the monoclinic fraction, attributable to recrystallization, or to total eradication of the monoclinic phase, attributable to melting. Thus, the monoclinic content is useful for characterizing the thermomechanical effects which the fibers have undergone; monoclinic melting predominates when ballistic penetration is complete. The predominant orthorhombic phase is generally reduced in mass fraction by the ballistic impact event.</p>	
<p>U.S. Army Materials Technology Laboratory Watertown, Massachusetts 02172-0001 X-RAY DIFFRACTION ANALYSIS OF CONTROL AND TEST FIBERS - C. Richard Desper</p>	<p>AD <u>UNCLASSIFIED</u> UNLIMITED DISTRIBUTION</p>
<p>Technical Report MTL TR 89-58, June 1989, 11 pp- illus.-tables, D/A Project: 1L161102.AH52</p>	<p>Key Words</p> <p>X-ray diffraction Body armor Filament fibers</p>
<p>A series of fabric test panels, test fired with a 17-grain fragment simulating projectile (FSP), of armor materials made from Spectra 1000 ("Allied-Signal Corporation) high tenacity polyethylene fibers were examined by wide-angle X-ray diffraction. A new procedure was developed for averaging out the orientation of fiber or fabric samples in order to yield data suitable for the determination of crystallinity. Data on the undamaged fabric show an average crystallinity of 0.65, with an orthorhombic fraction of 0.61, and the metastable monoclinic phase fraction at 0.04. Ballistic impact resulted at the damage zone in either an increase in the monoclinic fraction, attributable to recrystallization, or to total eradication of the monoclinic phase, attributable to melting. Thus, the monoclinic content is useful for characterizing the thermomechanical effects which the fibers have undergone; monoclinic melting predominates when ballistic penetration is complete. The predominant orthorhombic phase is generally reduced in mass fraction by the ballistic impact event.</p>	